

Filaments and Pancakes in the IRAS 1.2Jy Redshift Catalogue

B.S. Sathyaprakash¹, Varun Sahni², Sergei Shandarin³, Karl B. Fisher⁴

¹Department of Physics and Astronomy, Cardiff University of Wales, Cardiff, CF2 3YB, U.K.

²Inter-University Centre for Astronomy & Astrophysics, Post Bag 4, Ganeshkhind, Pune 411007, India

³Department of Physics and Astronomy, University of Kansas, Lawrence, KS 66045

⁴ Institute for Advanced Studies, Olden lane, Natural Sciences, Bldg E, Princeton, NJ 08540

ABSTRACT

We explore shapes of clusters and superclusters in the IRAS 1.2Jy redshift survey with three reconstructions spanning the range $\beta = 0.1, 0.5, 1.0$, where $\beta = \Omega^{0.6}/b$, b is the bias factor and Ω the present value of the dimensionless matter density. Comparing our results to Gaussian randomized reconstructions of the IRAS catalogue, we find structures having both planar and filamentary properties. For $\beta = 0.5, 1.0$ the *largest structures in the survey have a distinct tendency to be filament-like* in general agreement with the results of N-body simulations.

Redshift surveys of galaxies show that the large scale structure of the Universe has a non-random pattern which on different occasions has been described as being cellular, network-like, filamentary, a cosmic web etc. (Zeldovich, Einasto & Shandarin 1982, de Lapparent, Geller, & Huchra 1991, Bond, Kofman & Pogosyan 1996). It is also well known that individual structures forming through gravitational instability are likely to be anisotropic, since gravitational collapse leads generically to collapse along one dimension resulting in the formation of pancakes (Shandarin & Zeldovich 1989, Shandarin et al. 1995), moreover, with the passage of time, filamentary features acquire greater prominence and the large scale distribution develops a network like structure (Yess & Shandarin 1996, Sathyaprakash, Sahni & Shandarin 1996).

Geometrical properties of large scale structure have evoked great interest in recent years and mathematical tools as diverse as minimal spanning trees, genus curves, percolation theory, Minkowski functionals and shape statistics have all been employed in their study. The necessity of using different statistical measures to study large scale structure arises because traditional indicators of clustering such as the two-point correlation function, though robust, neither address the issue of ‘connectedness’ nor shape, issues which are central to an integral understanding of the morphology of large scale structure and of the physics of gravitational clustering (Sahni & Coles 1995).

Some key issues of the large scale clustering of matter, such as whether the Great Wall in the North and the Sculptor Wall in the South are truly one-dimensional ‘filaments’ or are part of a more complex cellular structure consisting of sheets and bubbles of which they represent a limited slice, will be addressed by upcoming large redshift surveys, such as the Sloan Digital Sky Survey (SDSS) and the 2 Degree Field (2dF). In the present paper, we report some progress towards this goal by analysing shapes of clusters and superclusters in the IRAS 1.2Jy redshift survey.

Percolation theory, when applied to gravitationally clustered systems, suggests that most of the matter is likely to be concentrated in pancakes, filaments and ribbons, since such an arrangement percolates easily (*i.e.*, at small values of the filling factor) as borne out by N-body simulations which show that the filling factor at percolation for CDM-type models can be as low as 3–5%, down from 16% for a Gaussian random field (Klypin & Shandarin 1993). Percolation analysis has also shown that the number of distinct clusters in a continuous density distribution peaks just before the onset of percolation. Thus, the percolation transition presents a natural threshold at which to study

the shapes of individual clusters (Sathyaprakash, Sahni & Shandarin 1996, Sathyaprakash, Sahni & Shandarin 1998) and in our study we shall employ this threshold to study clusters in the IRAS survey. (A comprehensive analysis of the IRAS 1.2Jy redshift survey using percolation theory was carried out in Yess, Shandarin & Fisher (1997).)

We shall analyse clusters in the IRAS 1.2Jy redshift survey using a moment-based shape statistic originally suggested for a distribution of points by Babul & Starkman 1992 (henceforth BS) and modified for use on continuous density distributions by Sathyaprakash, Sahni & Shandarin 1996. We briefly describe the modified version of the BS statistic below before applying it to clusters obtained at the percolation threshold using a nearest neighbors algorithm.

Let $\rho(\mathbf{x})$ be the density field of matter distribution defined on a grid with coordinates $\mathbf{x}^p = (x_1^p, x_2^p, x_3^p)$, $p = 1, \dots, N$. The first- and second-moments of the density distribution around a fiducial point \mathbf{x}^0 are given by

$$M_i(\mathbf{x}^0; R) = \frac{1}{\mathcal{M}} \sum_{p=1}^N y_i^p \rho(\mathbf{x}^p) W(|\mathbf{y}^p|), \quad (1)$$

$$M_{ij}(\mathbf{x}^0; R) = \frac{1}{\mathcal{M}} \sum_{p=1}^N y_i^p y_j^p \rho(\mathbf{x}^p) W(|\mathbf{y}^p|), \quad (2)$$

where $i, j = 1, 2, 3$, R is the radius of a window W centred on the point \mathbf{x}^0 , $\mathbf{y}^p \equiv \mathbf{x}^p - \mathbf{x}^0$ is the coordinate of the p th grid point relative to the fiducial point \mathbf{x}^0 , and \mathcal{M} is the total mass in a given region:

$$\mathcal{M} = \sum_{p=1}^N \rho(\mathbf{x}^p) W(|\mathbf{x}^p - \mathbf{x}^0|). \quad (3)$$

In this study we use a spherical top-hat window function. The moment of inertia tensor I_{ij} can be computed from the moments

$$I_{ij} = M_{ij} - M_i M_j. \quad (4)$$

The three eigenvalues, I_1 , I_2 and I_3 , of the inertia tensor are directly related to the three principal axes of an ellipsoid fitted to the distribution of matter around the given point (fitting by an ellipsoid becomes increasingly accurate in the limit of small R when the distribution can be approximated by a quadratic). Let us consider the ratios of the eigenvalues arranged in order of increasing magnitude, i.e., $I_1 > I_2 > I_3$:

$$\mu \equiv (I_2/I_1)^{1/2}, \quad \nu \equiv (I_3/I_1)^{1/2}, \quad (5)$$

The BS shape statistic consists of a triad of numbers (S_1, S_2, S_3) which can be constructed out of the parameters μ and ν as follows

$$S_1 = \sin \left[\frac{\pi}{2} (1 - \mu)^p \right], \quad S_2 = \sin \left[\frac{\pi}{2} a \right], \quad S_3 = \sin \left[\frac{\pi}{2} \nu \right], \quad (6)$$

where $p = \log 3 / \log 1.5$, the function $a(\mu, \nu)$ is implicitly given by

$$\frac{\mu^2}{a^2} - \frac{\nu^2}{a^2(1 - \alpha a^{1/3} + \beta a^{2/3})} = 1, \quad (7)$$

and $\alpha = 1.9$ and $\beta = -(7/8)9^{1/3} + \alpha 3^{1/3}$.

As a result $0 \leq S_i \leq 1$, $i = 1, 2, 3$, i.e., the BS statistic can be thought of as a vector whose components are *always* positive and whose magnitude never exceeds unity. A perfectly spherical distribution has $I_1 = I_2 = I_3$, implying $\mu = \nu = 1$, $a = 0$ and $(S_1, S_2, S_3) = (0, 0, 1)$. Similarly, for a planar distribution $I_1 = I_2$, $I_3 = 0$, which implies $\mu = 1$, $\nu = 0$ and $a = 1$, so that $(S_1, S_2, S_3) = (0, 1, 0)$. A distribution which is filamentary has $I_2 = I_3 = 0$, so that $\mu = \nu = a = 0$ and $(S_1, S_2, S_3) = (1, 0, 0)$. Thus, the three components of the *shape vector* $\mathbf{S} = (S_1, S_2, S_3)$

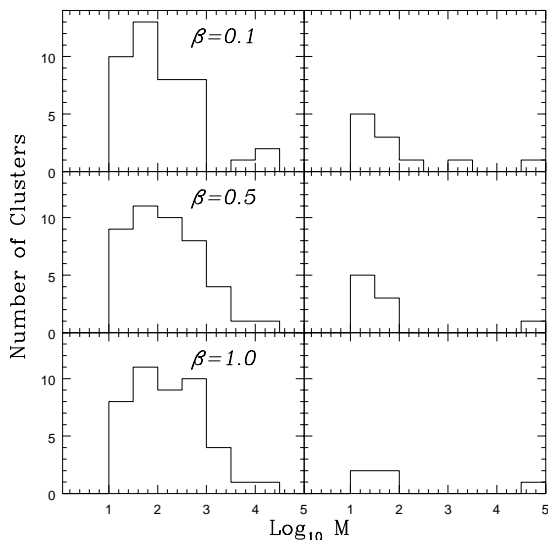


Fig. 1.— Multiplicity function of clusters in the IRAS 1.2 Jy red-shift catalogue (left). Also shown is the multiplicity function for a Gaussian randomisation of the IRAS catalogue (right).

represent filamentarity S_1 , planarity S_2 and sphericity S_3 . The magnitude and orientation of the shape vector describes some morphological properties of a distribution, for realistic distributions $S_i \neq 0$, $i = 1, 2, 3$. Since the three components of \mathbf{S} are related through and depend only on two parameters μ and ν , one can consider any two of them as being independent. In this work we shall mainly work with S_1 (linearity) and S_2 (planarity), small values of these two parameters imply a large value for sphericity S_3 .

We should point out that the moments in their present form can be used to determine shapes of continuous fields such as brightness/temperature or density distributions while those originally defined by BS could not have been used in such cases. We shall now apply them to study shapes in the IRAS 1.2 Jy redshift survey.

We now apply the BS shape statistic to overdense regions in a Wiener reconstruction of the IRAS 1.2 Jy redshift survey. The Wiener reconstruction method is useful in cosmology to construct a real space density field from a galaxy distribution in redshift space which may be incomplete and sparsely sampled. The Wiener reconstruction technique uses linear perturbation theory to model and compensate for redshift space distortions caused by peculiar velocities of galaxies. The latter depend upon the growth rate of the linear density contrast parametrised by $\beta = \Omega^{0.6}/b$ where Ω is the present value of the cosmic density parameter and b is the linear bias parameter (for details of Wiener reconstruction see Rybicki & Press (1992), Fisher et al. (1995a,b)). In this study we investigate a set of three reconstructions of the IRAS density field corresponding to $\beta = 0.1, 0.5, 1.0$. The real space density field is reconstructed on a 64^3 grid with side $200 h^{-1}$ Mpc ($20,000 \text{ km s}^{-1}$).

Clusters in the IRAS survey are identified using percolation theory and a ‘friends-of-friends’ algorithm on a grid using six nearest neighbors. A generic feature of any continuous density distribution (and therefore true also of the reconstructed IRAS density field) is that at very high thresholds only a small volume is in the overdense phase, so that the resulting number of clusters is very small and so is the volume in the largest cluster. As the density threshold is lowered, the number of clusters increases and the volume in the largest cluster grows rapidly due to merging of nearby clusters. At a critical value of the density (the *percolation threshold*) the largest cluster percolates, spanning the entire region of interest in a homogeneous sample. Further lowering of the threshold increases mergers, resulting in a subsequent decrease in the number of clusters. The total number of clusters, thus, peaks at thresholds close to percolation, making the percolation transition an objective and useful density threshold at which to study properties of individual clusters (Sathyaprakash, Sahni & Shandarin 1996, Sathyaprakash, Sahni

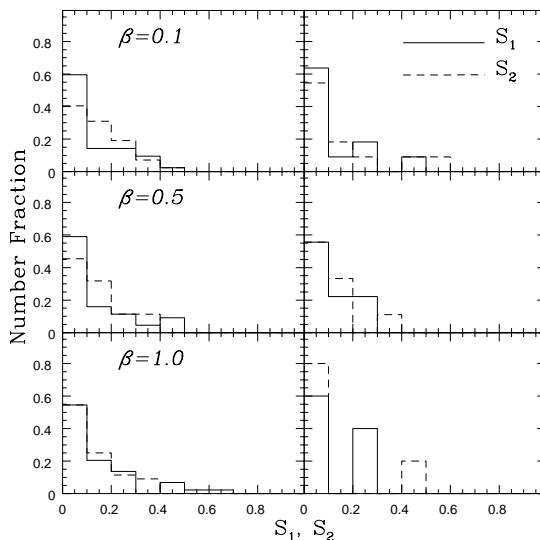


Fig. 2.— Shape-spectrum of IRAS clusters (left panels) and of the randomized catalogue (right panels).

& Shandarin 1998), and we shall use this threshold for studying cluster shapes in the IRAS survey.

The cluster multiplicity function for three reconstructions of the IRAS density field $\beta = 0.1, 0.5, 1.0$, is shown in Fig. 1 (left panels). Also shown are Gaussian randomized reconstructions of the IRAS catalogue, which serve as useful standards for our analysis (Fig. 1 right panels). In the IRAS catalogue there are between 40–50 clusters in each reconstruction. About half of them are small clusters a third are of intermediate mass and the rest are very massive. In a low Ω -Universe, or if the bias is very large, the clusters tend to be not as massive as in a high Ω -Universe or if there is no biasing. The randomized IRAS catalogue contains many small clusters, in Fig. 1 we only show clusters having volume larger than 8 grid cells, consequently, the randomized catalogue is seen to contain fewer large clusters than the IRAS catalogue, even though the total number of clusters in both catalogues is roughly the same. (Details of Gaussian randomisation of the IRAS density field can be found in Yess, Shandarin & Fisher 1997.)

In Fig. 2 we show the ‘shape-spectrum’ – the number fraction of IRAS clusters having a given value of the Babul and Starkman shape parameters S_1 & S_2 . From the shape-spectrum we see that most IRAS clusters are predominantly isotropic/spherical, however, a small fraction can have fairly large amounts of planarity/filamentarity. Fig. 2 does not provide a comprehensive picture since it weighs all clusters equally regardless of whether they are large or small. To explore the mass dependence of shape parameters we show the shape-mass histogram of IRAS density fields in Fig. 3. We find that for $\beta = 0.1$ clusters in all mass ranges have almost equal amounts of planarity and filamentarity. However, for $\beta = 0.5, 1.0$, the largest clusters (superclusters) tend to be predominantly filamentary, in agreement with the results of N-body simulations (Sathyaprakash, Sahni & Shandarin 1996, Sathyaprakash, Sahni & Shandarin 1998). (The statistical significance of these results is not yet clear due to the small number of such (large) objects in the IRAS survey volume.) Table is our catalogue of clusters in the IRAS density fields reconstructed with $\beta = 0.5$. (We do not include very small clusters having volume less than 8 grid cells.) We find several large clusters with significant amounts of filamentarity/planarity. It should be pointed out that the largest ‘percolating’ supercluster is likely to be ‘tree-like’ with several branches emanating from a ‘central trunk’. This will give it an isotropic appearance on very large scales. Since the BS statistic is moment-based it is likely to interpret such an isotropic structure as being spherical! This short coming of moment-based shape statistics can be avoided if one works with shape diagnostics based on Minkowski functionals as demonstrated in Sahni, Sathyaprakash & Shandarin 1998 and Sathyaprakash, Sahni & Shandarin 1998. (In addition, clusters occurring at the edge of the

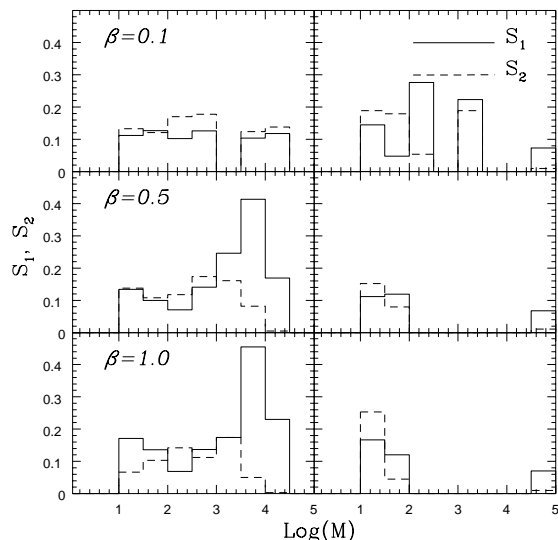


Fig. 3.— Shape-mass histogram of IRAS clusters (left panels) and of the randomized catalogue (right panels).

box may show enhanced planarity because of boundary effects.)

To conclude, we have addressed the issue of morphology of clusters and superclusters in the IRAS 1.2 Jy redshift catalogue. We find that individual clusters defined at the percolation threshold can have significant amounts of both filamentarity and planarity, the largest clusters appearing to be strongly filamentary. Although these results are broadly in agreement with recent studies of N-body simulations, their statistical implications are still unclear, mainly because of the sparseness of the IRAS catalogue. However, the stage is now set to analyse larger and deeper three-dimensional redshift surveys complementing the IRAS survey, such as the 2 Degree Field (2dF) and the Sloan Digital Sky Survey (SDSS). A comprehensive study of cluster and supercluster shapes in these surveys is bound to shed more light on the abundance of pancakes, filaments and ribbons and on the geometry of large scale structure, whether bubble-like, network-like or some other !

REFERENCES

- Babul, A. and Starkman, G.D. 1992 ApJ, 401, 28
 Bond, J.R., Kofman, L. & Pogosyan, D. 1996, Nature, 380, 603
 de Lapparent, V., Geller, M.J. & Huchra, J.P. 1991, ApJ, 369, 273
 Fisher, K.B., Lahav, O., Hoffman, Y., Lynden-Bell, D. & Zaroubi, S. 1995a, MNRAS, 272, 885
 Fisher, K.B., Huchra, J.P., Strauss, M.A., Davis, M., Yahil, A. & Schlegel, D. 1995b, ApJ Suppl., 100, 69
 Klypin, A.A. & Shandarin, S.F. 1993, ApJ, 413, 48
 Rybicki, G.B. & Press, W.H. 1992, Ap J, 398, 169
 Sahni, V., Sathyaprakash, B.S. & Shandarin, S.F. 1998, ApJ, 495, L5
 Sahni, V. & Coles, P. 1995, Physics Reports, 262, 1
 Sathyaprakash, B.S., Sahni, V. & Shandarin, S.F. 1996, ApJ, 462, L5
 Sathyaprakash, B.S., Sahni, V. & Shandarin, S.F. 1998, in preparation
 Shandarin S.F., Melott, A.L., McDavitt, A., Pauls, J.L., & Tinker, J. 1995, Phys. Rev. Lett., 75, 7
 Shandarin, S.F. & Zeldovich Ya. B. 1989, Rev. Mod. Phys., 61, 185

Yess, C. & Shandarin, S.F. 1996, ApJ, 465, 2

Yess, C., Shandarin, S.F. & K. Fisher 1997, ApJ, 474, 553

Zeldovich Ya. B., Einasto, J. & Shandarin, S.F. 1982, Nature, 300, 407

Table 1: Catalogue of clusters/superclusters from the IRAS reconstruction with $\beta = 0.5$. The list contains many interesting structures, some of them quite massive with significant amounts of planarity and/or filamentarity. (The first column is the cluster number (n), the second is volume in grid units (V , and the third mass/ 10^2 (M)

n	V	M	(S_1, S_2, S_3)
1	10927	238	(0.169, 0.005, 0.684)
2	1898	36	(0.413, 0.082, 0.375)
3	1417	27	(0.007, 0.388, 0.503)
4	905	17	(0.493, 0.024, 0.394)
5	775	15	(0.064, 0.221, 0.517)
6	494	10	(0.419, 0.012, 0.465)
7	302	5.3	(0.266, 0.199, 0.372)
8	302	5.1	(0.204, 0.266, 0.367)
9	287	4.9	(0.015, 0.104, 0.712)
10	232	4.4	(0.113, 0.128, 0.541)
11	252	4.2	(0.244, 0.271, 0.339)
12	239	4.2	(0.200, 0.024, 0.597)
13	208	3.5	(0.022, 0.376, 0.471)
14	197	3.3	(0.067, 0.027, 0.728)
15	161	3.0	(0.010, 0.051, 0.799)
16	165	2.8	(0.064, 0.007, 0.795)
17	123	2.0	(0.003, 0.107, 0.760)
18	117	1.9	(0.066, 0.189, 0.539)
19	108	1.8	(0.011, 0.293, 0.557)
20	97	1.6	(0.047, 0.114, 0.635)
21	97	1.6	(0.012, 0.017, 0.862)
22	93	1.5	(0.280, 0.020, 0.540)
23	85	1.4	(0.090, 0.239, 0.473)
24	73	1.2	(0.122, 0.148, 0.515)
25	48	0.78	(0.070, 0.188, 0.535)
26	38	0.78	(0.006, 0.016, 0.886)
27	44	0.74	(0.061, 0.019, 0.757)
28	37	0.59	(0.208, 0.180, 0.422)
29	31	0.56	(0.120, 0.016, 0.691)
30	32	0.53	(0.399, 0.011, 0.482)
31	25	0.40	(0.002, 0.180, 0.698)
32	24	0.39	(0.047, 0.179, 0.573)
33	21	0.38	(0.031, 0.047, 0.748)
34	23	0.37	(0.035, 0.349, 0.465)
35	21	0.35	(0.124, 0.003, 0.745)
36	17	0.27	(0.052, 0.379, 0.422)
37	17	0.27	(0.060, 0.024, 0.746)
38	16	0.27	(0.320, 0.004, 0.569)
39	16	0.27	(0.008, 0.040, 0.826)
40	15	0.25	(0.482, 0.066, 0.351)
41	14	0.22	(0.111, 0.190, 0.491)
42	11	0.18	(0.000, 0.117, 0.799)
43	10	0.16	(0.087, 0.117, 0.579)
44	9	0.14	(0.083, 0.302, 0.437)